229 nm UV LEDs on aluminum nitride single crystal substrates using p-type silicon for increased hole injection

Dong Liu, Sang June Cho, Jeongpil Park, Jung-Hun Seo, Rafael Dalmau, Deyin Zhao, Kwangeun Kim, Jiarui Gong, Munho Kim, In-Kyu Lee, John D. Albrecht, Weidong Zhou, Baxter Moody, and Zhenqiang Ma

Citation: Appl. Phys. Lett. **112**, 081101 (2018);
View online: https://doi.org/10.1063/1.5011180
View Table of Contents: http://aip.scitation.org/toc/apl/112/8
Published by the American Institute of Physics

229 nm UV LEDs on aluminum nitride single crystal substrates using p-type silicon for increased hole injection

Dong Liu,[1,a)] Sang June Cho,[1,a)] Jeongpil Park,[1,a)] Jung-Hun Seo,[1] Rafael Dalmau,[2] Deyin Zhao,[3] Kwangeun Kim,[1] Jiarui Gong,[1] Munho Kim,[1] In-Kyu Lee,[1] John D. Albrecht,[4,b)] Weidong Zhou,[3] Baxter Moody,[2] and Zhenqiang Ma[1,b)]

[1]*Department of Electrical and Computer Engineering, University of Wisconsin-Madison, Madison, Wisconsin 53706, USA*

[2]*HexaTech, Inc., 991 Aviation Parkway, Suite 800, Morrisville, North Carolina 27560, USA*

[3]*Department of Electrical Engineering, University of Texas at Arlington, 500 South Cooper Street, Arlington, Texas 76019, USA*

[4]*Department of Electrical and Computer Engineering, Michigan State University, 428 S. Shaw Lane, East Lansing, Michigan 48824, USA*

(Received 30 October 2017; accepted 7 February 2018; published online 20 February 2018)

AlGaN based 229 nm light emitting diodes (LEDs), employing p-type Si to significantly increase hole injection, were fabricated on single crystal bulk aluminum nitride (AlN) substrates. Nitride heterostructures were epitaxially deposited by organometallic vapor phase epitaxy and inherit the low dislocation density of the native substrate. Following epitaxy, a p-Si layer is bonded to the heterostructure. LEDs were characterized both electrically and optically. Owing to the low defect density films, large concentration of holes from p-Si, and efficient hole injection, no efficiency droop was observed up to a current density of 76 A/cm^2 under continuous wave operation and without external thermal management. An optical output power of 160 μW was obtained with the corresponding external quantum efficiency of 0.03%. This study demonstrates that by adopting p-type Si nanomembrane contacts as a hole injector, practical levels of hole injection can be realized in UV light-emitting diodes with very high Al composition AlGaN quantum wells, enabling emission wavelengths and power levels that were previously inaccessible using traditional p-i-n structures with poor hole injection efficiency. *Published by AIP Publishing.* https://doi.org/10.1063/1.5011180

Demand for ultraviolet (UV) light emitting diodes (LEDs) is increasing due to broad applications in biological and chemical detection, decontamination, medical treatment, high density optical recording, and lithography.[1–6] The group III-nitride material system is the most attractive candidate for UV LEDs spanning UVA, UVB, and UVC[7–14] owing to its wide bandgap range (GaN: 3.3 eV–AlN: ~6.2 eV). However, as the emission wavelength gets shorter, the external quantum efficiency (EQE) becomes significantly degraded.[15] Along with challenges in growth of high Al composition $Al_xGa_{1-x}N$ materials with low defect densities, the doping concentration limitations and high ionization energy of acceptors for wide gap AlGaN render the p-side of the diode structure quite resistive and the resulting hole injection efficiency is poor.[8] As a result of the insufficient hole injection, electron leakage ensues due to imbalance between electrons and holes, which is commonly addressed by the use of an electron blocking layer.[16] However, the EBL approach based on AlN ceases to be effective as the Al composition in the active quantum epistructures is high, reaching nearly 100%. In addition, achieving an Ohmic metal contact to typical p-layers with low contact resistance remains a critical limitation to obtaining an electrically efficient UVC LED. The approach used in this work overcomes both limitations.

A variety of approaches have been deployed to circumvent the fundamental p-type doping challenges, such as polarization doping[1,5,17,18] and tunnel junctions.[19–21] Both methods require careful control of precursor fluxes for grading the Al composition during the growth process, which complicates the epitaxy technique. We have reported a 237 nm UV LED using silicon as an efficient hole injector and postulated that shorter wavelength emission would be obtainable using this method.[22] In this paper, a 229 nm wavelength LED operating under continuous wave (CW) drive current is reported using a higher Al composition for the multi-quantum wells (MQWs).

The UV LED structure in Fig. 1(a) was grown on a bulk AlN substrate by low pressure organometallic vapor phase epitaxy (LP-OMVPE) in a custom high-temperature reactor. As shown in Fig. 1(a), following an initial 400 nm AlN homoepitaxial layer on an AlN substrate, a Si doped (concentration: 1×10^{19} cm^{-3}) 600 nm n-$Al_{0.7}Ga_{0.3}N$ contact and an electron injection layer were grown prior to the 3-period 3/6 nm $Al_{0.77}Ga_{0.23}N$/AlN MQW active region. The epitaxial growth was terminated with a 20 nm Mg doped (~4×10^{19} cm^{-3}) p-GaN layer to prevent rapid oxidation of the AlN surface, the challenges of which are explained elsewhere.[22] The dopant atomic concentration and free carrier concentration were characterized by secondary ion mass spectrometry (SIMS) and Hall Effect measurements, respectively. Prior to transferring a 100 nm thick, heavily doped single-crystal p-type Si nanomembrane (NM) with a doping concentration of 5×10^{19} cm^{-3}, a 0.5 nm thick Al_2O_3 layer, which acts as a quantum tunnel barrier and a passivation layer, was deposited by five cycles of an atomic layer deposition (ALD) process using an Ultratech/Cambridge Nanotech Savannah S200 ALD system.

[a)]D. Liu, S. J. Cho, and J. Park contributed equally to this work.

[b)]Authors to whom correspondence should be addressed: jalbrech@egr.msu.edu and mazq@engr.wisc.edu

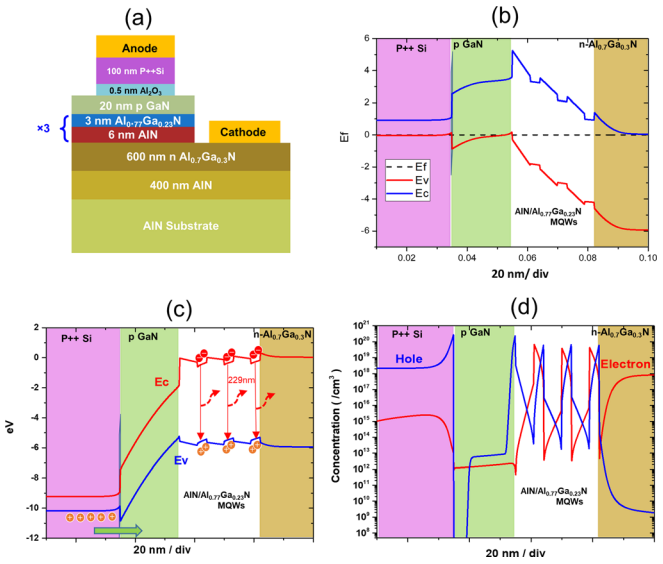

FIG. 1. (a) A schematic of the LED device structure. (b) Band diagram of the entire LED structure consisting of p-Si, p-GaN, i-$Al_{0.77}Ga_{0.23}N$/AlN MQWs, and n-$Al_{0.7}Ga_{0.3}N$ contact layer at equilibrium state and (c) under a forward bias of 10 V with 300 A/cm^2. (d) Carrier concentration distribution across the LED structure under forward bias.

Based on the previous analysis of the surface band bending and interface induced valence offset shift between the p-Si/Al_2O_3/p-GaN isotype heterojunction,[22] the whole LED structure is simulated using Silvaco®. The simulation input code is provided in the supplementary material. The band alignment across the LED structure under the thermal equilibrium state and forward bias (10 V) at 300 A/cm^2 is sketched in Figs. 1(b) and 1(c), respectively. As shown in Fig. 1(c), the sharp band bending of the p-GaN is a combined effect of polarization and applied electric field with the forward bias, which facilitates hole tunneling across the Si/GaN heterojunction and transport into the quantum well region. Reflected in the carrier concentration distribution plot in Fig. 1(d), a large quantity of holes from the reservoir of the p-type Si is injected into the $Al_{0.77}Ga_{0.23}N$ MQW region after tunneling through the thin oxide layer and drifting across the fully depleted p-type GaN layer.[22] As a result of the sufficient hole supply from Si, the concentration of electrons and holes is much better balanced within the quantum wells, which is essential to effective recombination rate and quantum efficiency. From direct radiative recombination of holes and electrons within the MQWs, 229 nm photons were generated, which corresponds to the emission from the 3 nm $Al_{0.77}Ga_{0.23}N$ QW energy states. A simulation control study is provided in the supplementary material to indicate the substantially increased hole concentration and increased radiative recombination rate in the MQW due to the use of p-type Si NM as a hole injector (Figs. S2–S7, supplementary material).

The device process flow is illustrated in Figs. 2(a)–2(g). The epitaxial samples [Fig. 2(a)] were cleaned prior to the Al_2O_3 layer deposition [Fig. 2 (b)]. Then, the p-type Si NM was transferred, followed by a rapid thermal anneal (RTA) at 500 °C for 5 min to increase the bonding strength between the p-type Si NM and Al_2O_3 [Fig. 2(c)] (Fig. S8 of the supplementary material for details of NM transfer and bonding). A mesa photoresist pattern was formed by photolithography image reversal, followed by a reactive ion etching (RIE) process to etch away Si and then etching p-GaN/AlN/$Al_{0.77}Ga_{0.23}N$/AlN MQW using an inductively coupled plasma (ICP) etcher [Fig. 2(d)]. Afterwards, the n-type $Al_{0.7}Ga_{0.3}N$ layer was exposed, and a metal stack (Ti/Al/Ni/Au: 15/100/50/250 nm) was deposited using optical photolithography patterning, e-beam evaporation, and liftoff processes. A thermal anneal at 950 °C for 30 s for the cathode contact was then performed [Fig. 2(e)]. Afterwards, the anode metal (Ti/Au: 15/100 nm) was deposited [Fig. 2(f)] in the same fashion of forming the cathode metal. Each device was isolated by etching away the Si NM and further down to the homoepitaxial AlN layer [Fig. 2(g)]. For optical characterization, the AlN substrate of the devices was thinned down to 80–100 μm. A fabricated device image is shown in Fig. 2(h). The cathode and anode metal contacts were designed to be in inter-digital form to minimize the lateral current spreading-induced resistance in the n-type $Al_{0.7}Ga_{0.3}N$ contact layer[23] (see supplementary material for details). In contrast, the sheet resistance of the 100-nm p-type Si NM with a doping concentration of 5×10^{19} cm^{-3} is negligible. Since the current passing through the MQW was primarily in the region beneath the anode, the effective device area was calculated from the anode metal area and was estimated to be 1.31×10^{-3} cm^2.

In order to realize substantial light output from LEDs, epitaxial layers with low threading dislocation densities and an atomically flat surface are highly desirable. Regarding these challenges, bulk AlN substrates were used in our work to grow Al-face high Al composition AlGaN epitaxial heterostructures, reducing the dislocation density by several orders of magnitude compared with layers on non-native substrates, as the epitaxial device layers inherit the low dislocation density ($<10^4$ cm^{-3}) of the single-crystalline bulk AlN.[24,25] Reducing surface roughness of the epitaxial layers is especially critical in our scenario with a foreign membrane transfer incorporated during fabrication. Surface roughness above ~2 nm leads to non-uniform bonding between the Si-NM and GaN, which hinders carrier transport across the Si/GaN interface, often resulting in leakage paths and reduced efficiency of the devices.

Given the crucial role of the surface roughness, we characterized the surface of the as-grown epitaxy samples and the epitaxy samples with the Al_2O_3 layer coated and p-type Si NM bonded using both an optical microscope and a Bruker Catalyst atomic force microscope (AFM). Figure 3(a)(i) shows a filtered optical microscopic image of the surface of the AlGaN sample. Figure 3(a)(ii) shows an AFM image of the epitaxial sample surface. The extracted AFM root-mean-square (RMS) surface roughness results marked in Fig. 3(a)(ii) were taken from a 2×2 μm^2 scan area. An averaged RMS roughness of 0.547 nm was measured, and the images show a crack-free surface. The smooth surface allowed the high-yield (100%) transfer of the Si NM to the epitaxy surface and also enabled intimate contact between the Si NM and the top GaN layer.

Figure 3(b)(i) shows a filtered optical microscopy image of a transferred p-Si NM on the Al_2O_3 deposited epitaxial sample. No wrinkles or defects were induced during the p-Si NM transfer. An AFM image of the surface of the transferred p-Si NM is shown in Fig. 3(b)(ii) with a 135×135 μm^2

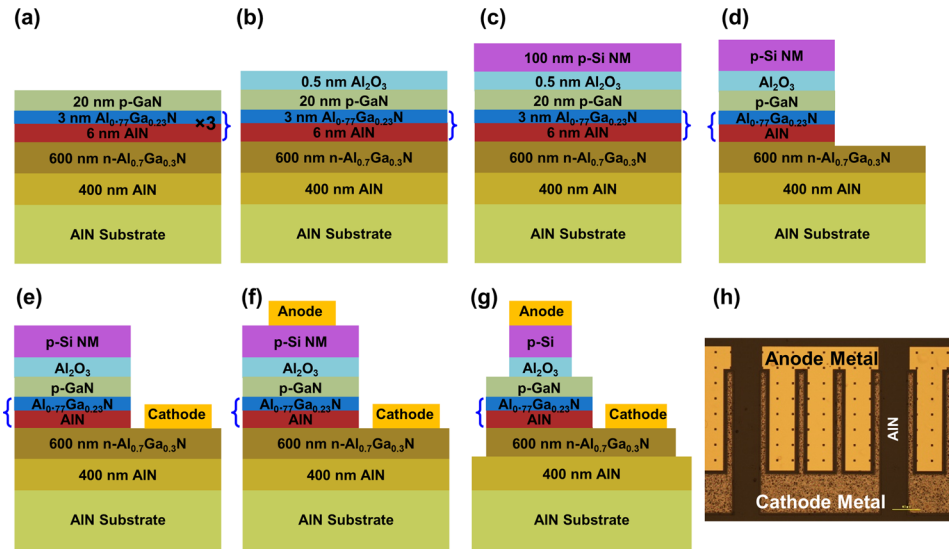

FIG. 2. UV LED fabrication process illustration. (a) Begin with a finished epitaxial sample. (b) Deposit 0.5 nm Al_2O_3 on the epitaxy sample. (c) Transfer and chemically bond 100 nm thick p-type Si NM. (d) Mesa etch down to n-type $Al_{0.7}Ga_{0.3}N$ layer. (e) Form cathode metal contact and thermal anneal. (f) Form anode contact metal. (g) Device isolation by etching down to the AlN substrate. (h) An optical microscopic image of a finished LED.

surface scan area. The averaged 0.677 nm RMS surface roughness values marked in Fig. 3(b)(ii) were extracted from a $2 \times 2\ \mu m^2$ scan. For reference, the RMS value of p-Si NM (before transfer) was measured as 0.121 nm with $2 \times 2\ \mu m^2$ AFM surface scan after NM was released from a silicon-on-insulator (SOI).[26] It is found that the surface roughness of Si NM after transfer roughly follows the original roughness of the epitaxy sample surface. The Al_2O_3 layer and Si NM are both rather thin and conformal and, therefore, inherit the surface roughness of the underlying epitaxial film.

To evaluate the electrical performance of the LEDs, current density as a function of applied voltage was measured. The measurement results are shown in Fig. 4(a). It is seen from the linear scale plot that the LED has a typical rectifying characteristic and a turn-on voltage of about 7 V. Besides the effective voltage dropped across the MQW region for carrier injection, the p-Si/p-GaN heterojunction, non-ideal n-contact, and lateral current spreading resistance in the n-AlGaN layer are responsible for part of the turn-on voltage as well. Additionally, although the reverse current is orders lower than the forward current, it is seen in the log scale plot that the reverse current is not trivial and well suppressed, which indicates the existence of wafer growth dislocation defects.[27] Electroluminescence (EL) spectra and optical power measurements were performed by coupling LED emission into a 6 inch diameter integrating sphere of a Gooch and Housego OL 770-LED calibrated spectroradiometer (see supplementary material for details). Note that the LED chip did not have any light extraction enhancements during EL measurements. Electrical power was supplied in the constant current mode and temperature is not controlled, so the LEDs were allowed to self-heat. The linear scale of

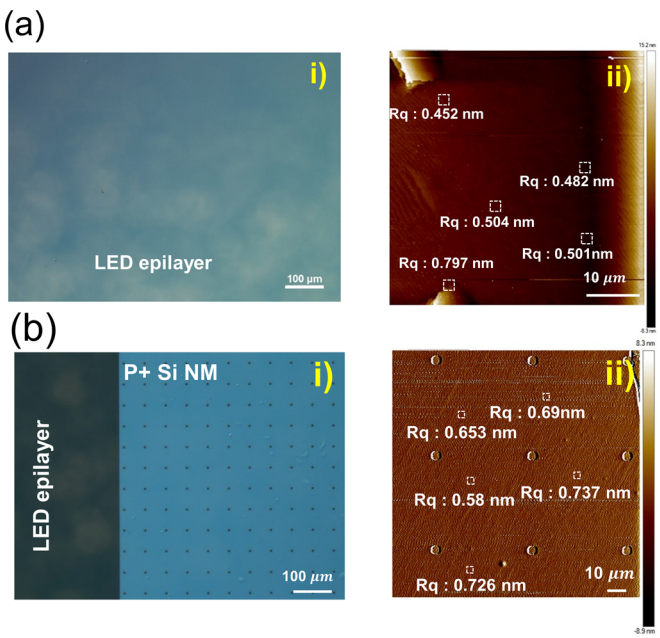

FIG. 3. Surface roughness characterizations. (a) LED epitaxy wafer before Si NM transfer: (i) A filtered optical microscopy image of cleaned epitaxy wafer. (ii) AFM images of a $50 \times 50\ \mu m^2$ scan area and RMS surface roughness with $2 \times 2\ \mu m^2$ AFM surface scan of the sample. (b) After p-type Si NM transfer on the Al_2O_3 deposited epitaxy sample: (i) Filtered microscopic image of p-type Si NM transferred on the Al_2O_3-coated epitaxy sample. (ii) AFM images of a $135 \times 135\ \mu m^2$ scan area and RMS surface roughness with $2 \times 2\ \mu m^2$ AFM surface scan of the sample.

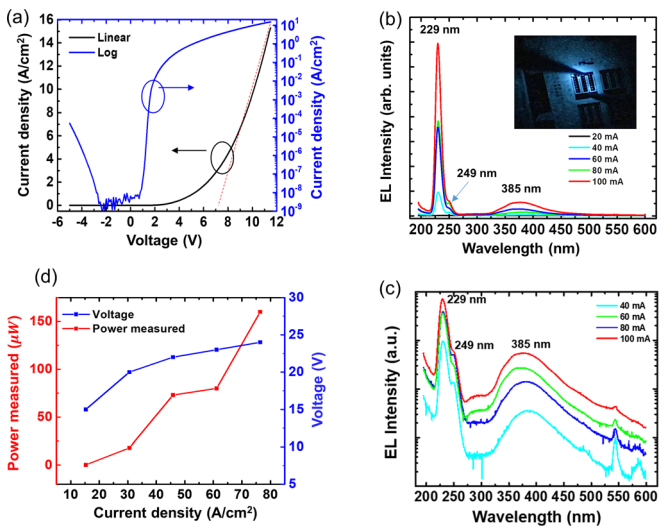

FIG. 4. (a) Current density-voltage characteristics of a typical LED on linear and log scales. (b) EL spectra under different driving current densities with CW operation. Inset: an optical microscopic image of the LED diode with forward bias applied showing visible blue illumination. (c) Logarithmic scale plot of EL spectra under currents of 40, 60, 80, and 100 mA. (d) Plot of measured light output power as a function of driving current density and the associated voltages.

the measured EL spectra for drive current varying from 20 mA to 100 mA is shown in Fig. 4(b). The 229 nm peak radiating from the MQWs is dominant, and with current ranging from 20 mA to 100 mA, the peak intensity increases correspondingly. To better illustrate the parasitic emission intensity in reference to the target peak, the logarithmic scale EL spectra under currents of 40, 60, 80, and 100 mA are plotted in Fig. 4(c). It is seen that the intensities of two parasitic peaks at 249 nm and 380 nm are both more than one order of magnitude lower than the main peak at 229 nm.

In addition to the main peak emission, there are two discernible weaker features at 249 nm and 385 nm in the UV and blue range, respectively. The former one is from the n-$Al_{0.7}Ga_{0.3}N$ layer with 4.98 eV gap energy, which corresponds to the emitted photon wavelength of 249 nm. Since the bandgap of the electron injection layer n-$Al_{0.7}Ga_{0.3}N$ is smaller than the photon energy generated by the MQWs consisting of $Al_{0.77}Ga_{0.23}N$/AlN, light emission at 229 nm is partially reabsorbed and leads to the secondary emission at 249 nm. The broad peak at 385 nm in the visible range has multiple contributions, likely from the top p-GaN combined and with deep-levels in AlGaN, excited by 229 nm photons. An optical microscopy image of a LED under current injection by probing is shown in the inset of Fig. 4(b) where blue emission is observed.

Optical output power was measured and, as seen in Fig. 4 (d), the output continuously increases with current density up to 76 A/cm^2, equivalent to 100 mA, and eventually reaches an output power intensity of 160 μW at 24 V bias. The nonlinearity of the power curve is suspected to be caused by the lack of thermal management of the LED. A higher light output power is expected by using light extraction patterning and by reducing losses to n-AlGaN. The corresponding external quantum efficiency (EQE) (see supplementary material for detailed calculations) was calculated to be 0.03%, which could be improved by further thinning down the AlN substrate, which induces substantial absorption around the 229 nm wavelength range due to point defects in the substrate.[28] The comparisons of the EQE values and the light output power levels of our work with others can be found in the supplementary material (Fig. S1).

In summary, we have demonstrated a 229 nm AlN/$Al_{0.77}Ga_{0.23}N$ MQW LED with a p-type Si NM as both a p-contact and a hole injection layer for high Al composition MQW structures. The light emission at 229 nm showed no significant efficiency droop up to 76 A/cm^2 in CW operation and without thermal management. This study provides evidence that UVC emission from electrically injected diode structures enabled by p-type Si NM hole injection layers is a promising approach for the practical implementation of UVC LEDs and may provide a route to diode lasers in the future.

See supplementary material for (1) complete Silvaco input code; (2) EL measurement and EQE calculations; (3) control study compared with no Si UV LED; (4) detailed Si NM bonding process; and (5) thermal anneal effects on Si NM.

We acknowledge the support of the Defense Advanced Research Projects Agency (HR0011-15-2-0002). The program manager is Dr. Daniel Green.

[1]J. Simon, V. Protasenko, C. Lian, H. Xing, and D. Jena, Science **327**, 60 (2010).
[2]J. Verma, P. K. Kandaswamy, V. Protasenko, A. Verma, H. Xing, and D. Jena, Appl. Phys. Lett. **102**, 041103 (2013).
[3]Y. Taniyasu and M. Kasu, Appl. Phys. Lett. **99**, 251112 (2011).
[4]J. Verma, S. M. Islam, V. Protasenko, P. Kumar Kandaswamy, H. Xing, and D. Jena, Appl. Phys. Lett. **104**, 021105 (2014).
[5]S. M. Islam, K. Lee, J. Verma, V. Protasenko, S. Rouvimov, S. Bharadwaj, H. Xing, and D. Jena, Appl. Phys. Lett. **110**, 041108 (2017).
[6]J. Carrano, http://go.nature.com/JNBVGN for DARPA (2005).
[7]J. P. Zhang, M. A. Khan, W. H. Sun, H. M. Wang, C. Q. Chen, Q. Fareed, E. Kuokstis, and J. W. Yang, Appl. Phys. Lett. **81**, 4392 (2002).
[8]Y. Taniyasu, M. Kasu, and T. Makimoto, Nature **441**, 325 (2006).
[9]J. W. Orton and C. T. Foxon, Rep. Prog. Phys. **61**, 1 (1998).
[10]H. Hirayama, N. Noguchi, T. Yatabe, and N. Kamata, Appl. Phys. Express **1**, 051101 (2008).
[11]H. Hirayama, N. Noguchi, and N. Kamata, Appl. Phys. Express **3**, 032102 (2010).
[12]T. Nishida, H. Saito, and N. Kobayashi, Appl. Phys. Lett. **79**, 711 (2001).
[13]H. Hirayama, N. Maeda, S. Fujikawa, S. Toyoda, and N. Kamata, Jpn. J. Appl. Phys., Part 2 **53**, 100209 (2014).
[14]C. Pernot, S. Fukahori, T. Inazu, T. Fujita, M. Kim, Y. Nagasawa, A. Hirano, M. Ippommatsu, M. Iwaya, S. Kamiyama, I. Akasaki, and H. Amano, Phys. Status Solidi A **208**, 1594 (2011).
[15]M. Kneissl and J. Rass, *III-Nitride Ultraviolet Emitters* (Springer International Publishing, Switzerland, 2016).
[16]F. Mehnke, C. Kuhn, M. Guttmann, C. Reich, T. Kolbe, V. Kueller, A. Knauer, M. Lapeyrade, S. Einfeldt, J. Rass, T. Wernicke, M. Weyers, and M. KneisslM, Appl. Phys. Lett. **105**, 051113 (2014).
[17]O. Ambacher, B. Foutz, J. Smart, J. R. Shealy, N. G. Weimann, K. Chu, M. Murphy, A. J. Sierakowski, W. J. Schaff, L. F. Eastman, R. Dimitrov, A. Mitchell, and M. Stutzmann, J. Appl. Phys. **87**, 334 (2000).
[18]Z. Peng, L. Shi-Bin, Y. Hong-Ping, W. Zhi-Ming, C. Zhi, and J. Ya-Dong, Chin. Phys. Lett. **31**, 118102 (2014).
[19]S. M. Sadaf, S. Zhao, Y. Wu, Y. H. Ra, X. Liu, S. Vanka, and Z. Mi, Nano Lett **17**, 1212 (2017).
[20]Y. Zhang, S. Krishnamoorthy, J. M. Johnson, F. Akyol, A. Allerman, M. W. Moseley, A. Armstrong, J. Hwang, and S. Rajan, Appl. Phys. Lett. **106**, 141103 (2015).
[21]A. G. Sarwar, B. J. May, J. I. Deitz, T. J. Grassman, D. W. McComb, and R. C. Myers, Appl. Phys. Lett. **107**, 101103 (2015).
[22]S. J. Cho, D. Liu, J.-H. Seo, R. Dalmau, K. Kim, J. Park, D. Zhao, X. Yin, Y. H. Jung, I.-K. Lee, M. Kim, X. Wang, J. D. Albrecht, W. Zhou, B. Moody, and Z. Ma, preprint arXiv:1707.04223 (2017).
[23]H. Rodríguez, N. Lobo, S. Einfeldt, A. Knauer, M. Weyers, and M. Kneissl, Phys. Status Solidi A **207**, 2585–2588 (2010).
[24]R. Dalmau, B. Moody, R. Schlesser, S. Mita, J. Xie, M. Feneberg, B. Neuschl, K. Thonke, R. Collazo, and A. Rice, J. Electrochem. Soc. **158**, H530 (2011).
[25]T. Wunderer, C. Chua, J. Northrup, Z. Yang, N. Johnson, M. Kneissl, G. Garrett, H. Shen, M. Wraback, B. Moody, H. S. Craft, R. Schlesser, R. F. Dalmau, and Z. Sitar, Phys. Status Solidi C **9**, 822 (2012).
[26]K. Zhang, J.-H. Seo, W. Zhou, and Z. Ma, J. Phys. D: Appl. Phys. **45**, 143001 (2012).
[27]R. Dalmau, B. Moody, J. Xie, R. Collazo, and Z. Sitar, Phys. Status Solidi A **208**, 1545–1547 (2011).
[28]R. Collazo, J. Xie, B. E. Gaddy, Z. Bryan, R. Kirste, M. Hoffmann, R. Dalmau, B. Moody, Y. Kumagai, and T. Nagashima, Appl. Phys. Lett. **100**, 191914 (2012).